

Synthesis and Characterization of Fluorescent Polymer - Single-Walled Carbon Nanotube Complexes with Charged and Noncharged Dendronized Perylene Bisimides for Bioimaging Studies

Katharina Huth,[‡] Mareen Gläske,[‡] Katharina Achazi, Georgy Gordeev, Shiv Kumar, Raúl Arenal, Sunil K. Sharma, Mohsen Adeli, Antonio Setaro, Stephanie Reich, and Rainer Haag**

K. Huth, Dr. K. Achazi, Prof. M. Adeli, Prof. M. Adeli, Prof. R. Haag
Institute of Chemistry and Biochemistry, Freie Universität Berlin, Berlin 14195, Germany
E-mail: haag@zedat.fu-berlin.de

M. Gläske, G. Gordeev, Dr. A. Setaro, Prof. S. Reich
Department of Physics, Freie Universität Berlin, Berlin 14195, Germany
E-mail: setaro@zedat.fu-berlin.de

Dr. S. Kumar, Prof. S. K. Sharma
Department of Chemistry, University of Delhi, Delhi 110 007, India

Dr. R. Arenal
Institute of Nanoscience of Aragon (INA), Advanced Microscopy Laboratory (LMA),
University of Zaragoza, Zaragoza 50018, Spain
Foundation ARAID, Zaragoza 50018, Spain

Prof. M. Adeli
Department of Chemistry, Faculty of Science, Lorestan University, Khorram Abad 68151-44316, Iran.

[‡] These authors contributed equally.

Keywords: Single-walled carbon nanotubes (SWNTs), perylene bisimide, bioimaging, cytocompatibility, optical window

Fluorescent nanomaterials are expected to revolutionize medical diagnostic, imaging, and therapeutic tools due to their superior optical and structural properties. Their inefficient water solubility, cell permeability, biodistribution, and high toxicity, however, limit the full potential of their application. Here we introduce a water-soluble, fluorescent, cytocompatible polymer-single-walled carbon nanotube (SWNT) complex for bioimaging applications to overcome these obstacles. The supramolecular complex consists of an alkylated polymer conjugated with neutral hydroxylated or charged sulfated dendronized perylene bisimides (PBIs), and SWNTs as a general immobilization platform. The polymer backbone solubilizes the SWNTs, decorates them with fluorescent PBIs, and strongly improves their cytocompatibility by wrapping around the SWNT scaffold. In photophysical measurements and biological *in vitro* studies, sulfated complexes exhibit superior optical properties, cellular uptake, and intracellular staining over

their hydroxylated analogs. A toxicity assay confirmed the highly improved cytocompatibility of our polymer-wrapped SWNTs towards surfactant-solubilized SWNTs. In microscopy studies the complexes allowed for the direct imaging of the SWNTs' cellular uptake via the PBI and SWNT emission using the 1st and 2nd optical window for bioimaging. These findings render our polymer-SWNT complexes with nanometer size, dual fluorescence, multiple charges, and high cytocompatibility as valuable systems for a broad range of fluorescent imaging studies.

1. Introduction

Single-walled carbon nanotubes (SWNTs) are nanoscale carbon cylinders with remarkable characteristics including high mechanical robustness, efficient thermal conduction, and outstanding electronic and optical properties. Their long and hollow structure provides a stable platform for the immobilization of molecules in high local concentrations and offers the possibility to introduce multiple functions on one tube.^[1-2] These features make them particularly popular in biomedical applications like cancer therapeutics, tissue engineering, bioimaging, or DNA, protein, and virus detection.^[3] Recently, it was shown that cancer cells can be detected, visualized, and treated by inserting only one theranostic SWNT complex with three different functions including reporter molecules, contrast agents, and pharmaceutical drugs for multimodal drug delivery.^[1]

The emission of the SWNTs in the near infrared (NIR) makes them attractive candidates for biological imaging studies. The transparency window of biological tissue is located in the range from 650 to 1350 nm with the 1st optical window (650 to 950 nm) matching the excitation range of SWNTs and the 2nd optical window (1000 to 1350 nm) matching the emission range of SWNTs.^[4] However, their poor solubility, high toxicity, and low fluorescence quantum yield (FQY, below 1%) has hampered them from extensive use in biomedical applications.^[5-7] Several attempts have been made to debundle SWNTs and increase their FQYs. Bile salt

surfactants debundle SWNTs and increase their FQY but at cost of their biocompatibility.^[8] Noncovalent PEGylation promotes the biocompatibility of nanotubes but compromises their already low FQY.^[8] Combining the two approaches, Welsher *et al.* found a way to retain the FQY by first solubilizing SWNTs with sodium cholate under subsequent replacement of the surfactant with phospholipid-PEG.^[9-10] The use of nanoplasmonic colloids represents another promising way to increase the FQY by enhancing the SWNT emission;^[11] but generally FQYs remain low compared to common fluorescent dyes such as cy3 (4%),^[12] rhodamine (12%),^[13] or bodipy (4%)^[14] typically used in fluorescence microscopy.

Perylene bisimides (PBIs) possess excellent properties for bioimaging purposes such as high chemical and photophysical stability, outstanding fluorescence properties, and a long emission wavelength.^[15-16] They have been versatilely employed as fluorescent labels,^[17-21] membrane markers,^[22-23] or anti-inflammatory agents.^[24] The striking photostability^[15-16] of PBI expressed in long fluorescence lifetimes of approximately 4 to 5 ns^[25-29] and monoexponential fluorescence decays over at least 16 ns^[28-30] becomes obvious in comparison to other conventional fluorescent probes^[31] such as cy5 (0.91 ns), alexa fluor 647 (1.04 ns), and rhodamine B (1.74 ns) with significantly lower lifetimes. The superior long-term photostability of PBI compared to common fluorophores like coumarin or fluorescein was recently demonstrated in a study by Zimmerman *et al.*,^[32] additionally, they were able to improve the FQYs of PBIs by side-isolation of the fluorophore in the imide positions. However, a major drawback of PBI-based dyes is their aggregation tendency in aqueous solution caused by the polyaromatic scaffold of the PBI cores resulting in fluorescence quenching. Charged groups have been introduced in the bay-regions^[33] or imide positions^[17, 24] to overcome the aggregation behavior and preserve their fluorescence properties with FQYs up to 100%. However, charged dyes inevitably raise the concern of nonspecific binding through electrostatic interactions with ionic cell components when being applied in bioimaging.^[15-16] Negatively charged fluorophores

often lack cell permeability through repulsive interactions with the negative cell membrane^[34-35] or undergo undesired attractive interactions with positive cell components like nuclear proteins^[36-37] resulting in limited uptake or nonspecific distribution, respectively. Molecular recognition on the other hand relies on specific attractive or repulsive interactions between two partner molecules. Therefore, charge may also be favorable to trigger cellular uptake via receptor-mediated endocytosis^[38] or targeted binding through electrostatic interactions.^[16]

Rationally designed perylenes derivatives have proven to be highly effective surfactants in debundling and isolating SWNTs when bearing a dendritic hydrophilic structure as solubilizing moiety and a hydrophobic aliphatic tail as an adhesive unit for the SWNTs.^[39-46] A cytotoxicity study of SWNTs solubilized with a perylene surfactant or with a commercial biological surfactant showed comparable results confirming the good cytocompatibility of the perylene-functionalized SWNTs.^[47] However, the immobilization of those functional perylene surfactants onto the surface of SWNTs can result in energy or charge transfer processes between the π -conjugated systems quenching the perylene emission.^[48] Hirsch *et al.* observed a charge transfer between the dye and SWNTs accompanied by a strong quenching of the PBI by a factor of > 100 .^[41] Ernst *et al.* observed highly efficient energy transfer from the perylene to the tubes at the cost of the perylene luminescence quenched by a factor of 10^4 .^[49] The risk of unwanted dye-tube interactions makes perylene surfactants unfavorable for bioimaging applications. We circumvented this issue by employing polymer wrapping as an alternative functionalization method that should minimize dye-tube interactions and, thus, prevent dye quenching.

Polymers are attractive dispersing agents for SWNTs because they can wrap around the SWNT backbones attaching different functional moieties onto their sidewalls.^[50-54] The well-established polymer wrapping method benefits from the tight and uniform enclosure of the SWNTs by the polymer, which endures filtration processes, modification of pH, and other

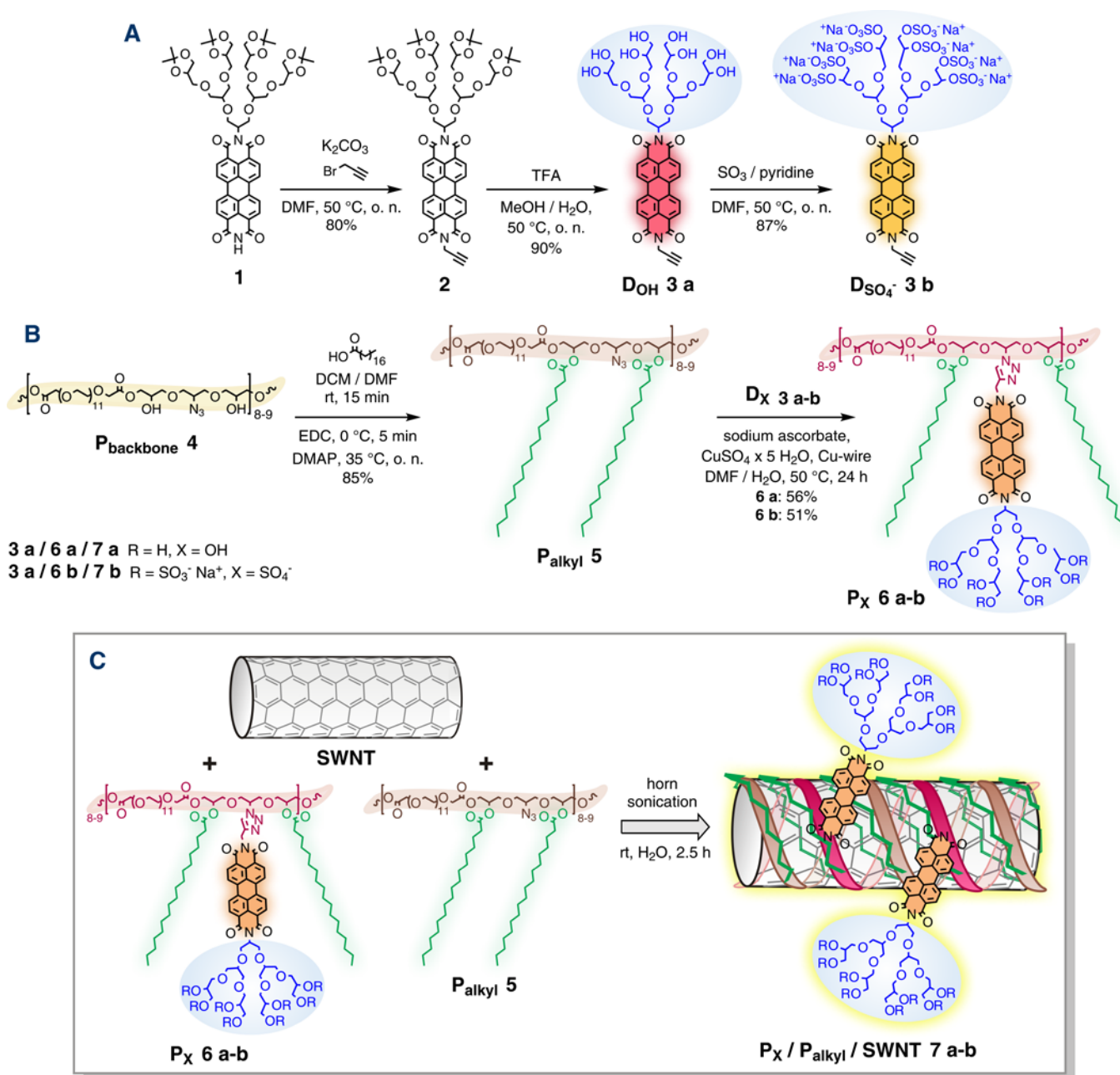
environmental changes.^[55-56] Polymer-wrapping not only preserves the photoluminescence of SWNTs, but also increases their sensitivity, making polymer-functionalized SWNTs suitable building blocks for biosensors.^[57-58] In addition, polymers promote the biocompatibility of SWNTs by shielding their backbones.^[59-62] We hypothesized that the functionalization of SWNTs with dendronized PBIs on alkylated polymers would result in water-soluble, individualized, and biocompatible SWNT complexes applicable for bioimaging studies. Benefiting from the high brightness of ionically charged systems, we sought to improve the FQYs of PBI by introducing charged groups on the dendritic head groups. The combination of PBI fluorophores emitting in the visible range and intrinsically fluorescent SWNTs emitting in the NIR creates a dual fluorescent system, which should allow the imaging in the 1st and 2nd optical transparency window of tissue. The concept of dual (visible and NIR) imaging by fluorescently labeled polymers on intrinsically fluorescent SWNTs has recently been demonstrated by other work groups, whose nanoconstructs provided good guidance for the design of our multifunctional complexes.^[63-66]

In the present study, we employed polymer-functionalized SWNTs with bright PBI fluorophores as cytocompatible SWNT complexes for potential bioimaging applications. The polymer wrapping method allows a helically wrapped alignment of the polymer-conjugated PBIs around the SWNTs inhibiting luminescence-reducing energy transfer or dye stacking.^[67] We used an amphiphilic C₁₈-alkylated polymer equipped with a 2nd-generation [G2] oligoglycerol (OG) dendronized PBI dye to functionalize the SWNTs. Each component of the complex system fulfills a certain purpose: i) the alkyl chains ensure hydrophobic interactions with the SWNT scaffold, ii) the cytocompatible polymer solubilizes and coats the toxic tubes, iii) the OG dendron introduces hydrophilicity and prevents dye quenching, iv) the PBI serve as a fluorescent label, and v) the SWNTs are the basic immobilization scaffold. To further avoid fluorescence quenching aggregation and promote receptor-mediated cellular uptake, we

introduced negative ionic charges on the dendron via a simple sulfation procedure. The neutral hydroxylated and charged sulfated SWNT complexes were prepared in a six-step synthesis and photophysically characterized by absorption and emission spectroscopy. *In vitro* toxicity and uptake studies on HeLa cells showed that our multifunctional complex drastically improves the cytocompatibility of SWNTs and allows for the direct imaging of their cellular uptake in two optical windows. Comparison between the charge neutral and negatively charged SWNT complexes showed that charged species have superior cellular uptake and staining properties than their neutral analogs.

2. Results and Discussion

2.1 Synthesis and Characterization



Scheme 1. General synthetic strategy for polymer-SWNT complexes comprising the following steps: A) dye synthesis of hydroxylated and sulfated OG-dendronized PBIs **D_x 3 a-b**, B) polymer preparation via alkylation and dye conjugation of **P_{backbone} 4** leading to dye polymers **P_x 6 a-b** via intermediate native polymer **P_{alkyl} 5**, and C) complex formation by sonication in aqueous solution leading to the final polymer-SWNT complexes **P_x / P_{alkyl} / SWNT 7 a-b** in a hydroxylated and sulfated version with X = OH or SO₄⁻ as functional groups in the dendron periphery. The schematic representation of the final complex **P_x / P_{alkyl} / SWNT** describes an idealized arrangement of the polymers around the tubes by helical wrapping.

The synthesis of the hydroxylated and sulfated polymer-functionalized SWNTs **7 a-b** was carried out in three major steps: A) synthesis of the dendronized PBI dyes, B) preparation of the dye-conjugated polymers, and C) formation of the polymer-SWNT complexes as shown in Scheme 1. For the preparation of the free dyes, OG-dendronized propargylated PBIs were synthesized in a charged and a noncharged version. The propargylation of previously reported mono imide-substituted [G2]-dendronized PBI **1**^[17] gave protected organo-soluble PBI **2**. Subsequent acid-catalyzed hydrolysis of the isopropylidene protecting groups with trifluoroacetic acid (TFA) afforded water-soluble monofunctional **D_{OH} 3 a**. The hydroxylated dendron was sulfated with a sulfur trioxide pyridine complex at moderate temperatures in dry DMF which led to charged **D_{SO₄⁻}** **3 b** after counter ion exchange from pyridinium to sodium ions by ultrafiltration.^[68] The successful substitution was confirmed by elemental analysis with a 99.8% degree of sulfation. Linear polyethylene glycol (PEG) and triglycerol based polymer **P_{backbone} 4**^[69] were synthesized according to a reported procedure with a degree of polymerization of 8.5 monomer units per polymer used to calculate the molecular weights (see polymer synthesis, ESI). Subsequent alkylation of the secondary hydroxyl groups with stearic acid via a Steglich-type esterification afforded grafted block copolymer **P_{alkyl} 5** in good yields. Click coupling between propargylated free dyes **D_x 3 a-b** and azide-carrying **P_{alkyl}** gave dye-conjugated polymers **P_x 6 a-b** in a charge neutral hydroxylated (X = OH) and ionically changed sulfated (X = SO₄⁻) version, which were subjected to ultra, gel, and centrifugal filtration to remove catalyst remains and unreacted free dyes.^[70-71] The complete conversion of the click reaction was monitored by the disappearance of the azide band at $\approx 2100\text{ cm}^{-1}$ in the IR spectra. The dyes and polymers were characterized by ¹H and ¹³C NMR spectroscopy (Figure S1-S9, ESI), mass spectrometry, and IR (Figure S10, ESI). The final polymer-functionalized SWNT complexes were prepared by horn sonication in aqueous solution to ensure efficient

solubilization and debundling of the tubes. In the first step, SWNTs (0.1 g L^{-1}) were wrapped with dye polymer ensuring a PBI concentration of $10 \text{ }\mu\text{M}$ (corresponds to a dye polymer \mathbf{P}_X concentration of $1.18 \text{ }\mu\text{M}$). In the second step, native polymer $\mathbf{P}_{\text{alkyl}}$ ($130 \text{ }\mu\text{M}$) was added to the mixture to improve the debundling of the tubes while maintaining a constant dye concentration giving a $\mathbf{P}_X / \mathbf{P}_{\text{alkyl}}$ molar ratio of approximately 1 : 11. The final supramolecular polymer-SWNT complexes denoted as $\mathbf{P}_X / \mathbf{P}_{\text{alkyl}} / \text{SWNT } \mathbf{7 a-b}$ were characterized by high resolution transmission electron microscopy (HRTEM) and electron loss spectroscopy (EELS), which confirmed the complex formation of the sulfated representative as seen in Figure S15.

To get insight into the polymer properties, molecular weight, charge, size, and aggregation studies by gel permeation chromatography (GPC), zeta potential, and dynamic light scattering (DLS) were performed (see Table S1 and Figures S11 and S12, ESI). The polymers feature calculated molecular weights and narrow polydispersity indices (PDIs) of 20 kDa and 1.1 for \mathbf{P}_{OH} and slightly higher values of 27 kDa and 1.4 for $\mathbf{P}_{\text{SO}_4^-}$. Surface charge analysis confirmed the mainly neutral potential of hydroxylated \mathbf{P}_{OH} (-4.2 mV) and strongly negative potential of sulfated $\mathbf{P}_{\text{SO}_4^-}$ (-33 mV) in 0.1 M phosphate buffer at pH 7.4. Since a small, absolute zeta potential of nanoparticles implies a rapid aggregation,^[72] the strongly negative potential of $\mathbf{P}_{\text{SO}_4^-}$ suggests a better monomerization of the polymers. Native polymer $\mathbf{P}_{\text{alkyl}}$ features a large hydrodynamic diameter of $> 100 \text{ nm}$ due to the poor solubility of the attached alkyl chains, however, the hydrophobic character is advantageous for the SWNT isolation via hydrophobic interactions. The solubilizing effect of the OG dendrons becomes evident by reducing the diameter by a factor of ~ 10 after the dye conjugation to the polymer. The diameter of sulfated $\mathbf{P}_{\text{SO}_4^-}$ (17.3 nm) is slightly larger than that of its hydroxylated analog \mathbf{P}_{OH} (12.6 nm), presumably due to the repulsion forces of the sulfate groups, which increase the overall sterical demand of polysulfated compounds. To investigate the tendency of aggregation of charged vs.

noncharged species, the critical aggregation concentration^[73] (CAC) was determined via DLS. Consistent to the charge and size results, **P**_{SO₄⁻ provides a higher CAC than its hydroxylated counterpart **P**_{OH}, which proves the superior aggregation suppression of ionically charged species. The free dyes behave similarly to the dye polymers with higher molecular weight, charge, size, and aggregation properties for charged rather than for noncharged dyes.}

2.2 Photophysical Characterization

For potential biological applications of the SWNT complexes, their photophysical properties were analyzed by absorption and emission spectroscopy in aqueous solution. To gain insight into the effect of charge and conjugation, prior concentration-dependent measurements of the hydroxylated and sulfated free dyes **D**_X and polymers **P**_X (X = OH or SO₄⁻) were conducted. The study revealed that neutral dyes have a concentration-dependent aggregation behavior while charged dyes have a concentration-independent monomeric behavior (see Figure S13, ESI). Taking these findings into account, we examined the polymer-SWNT complexes at a constant dye concentration of 1 μM in aqueous solution. To consider possible optical changes of the PBIs due to the usage of the native polymer, the free dyes **D**_X, dye-conjugated polymers **P**_X, and SWNT complexes were investigated separately and in mixtures with native polymer **P**_{alkyl}. The corresponding spectra are shown in Figure 1 and the related spectroscopic data are listed in Table S2.

The absorption spectra of the PBI-based compounds reveal a band shape ranging from 400 to 650 nm with two intense bands at 535 nm ($S_0 \rightarrow S_0$) and 500 nm ($S_0 \rightarrow S_1$) and a less pronounced band at 470 nm ($S_0 \rightarrow S_2$) belonging to the stated electronic transitions. The location of the absorption maximum provides evidence about the aggregation state of the dye. While a maximum located at the short wavelength peak around 500 nm points to the presence of face-to-face stacked H-type aggregates,^[74-77] a red-shifted maximum at the long wavelength

peak around 535 nm indicates the presence of isolated PBI monomers. In addition to the band shape, the extent of aggregation can be measured by the different peak ratios between the first and the second absorption maximum denoted as A^{0-0}/A^{0-1} with a value of ≈ 1.6 for monomeric and ≤ 0.7 for strongly aggregated core-unsubstituted PBIs in water.^[17, 24, 78-81] To determine the

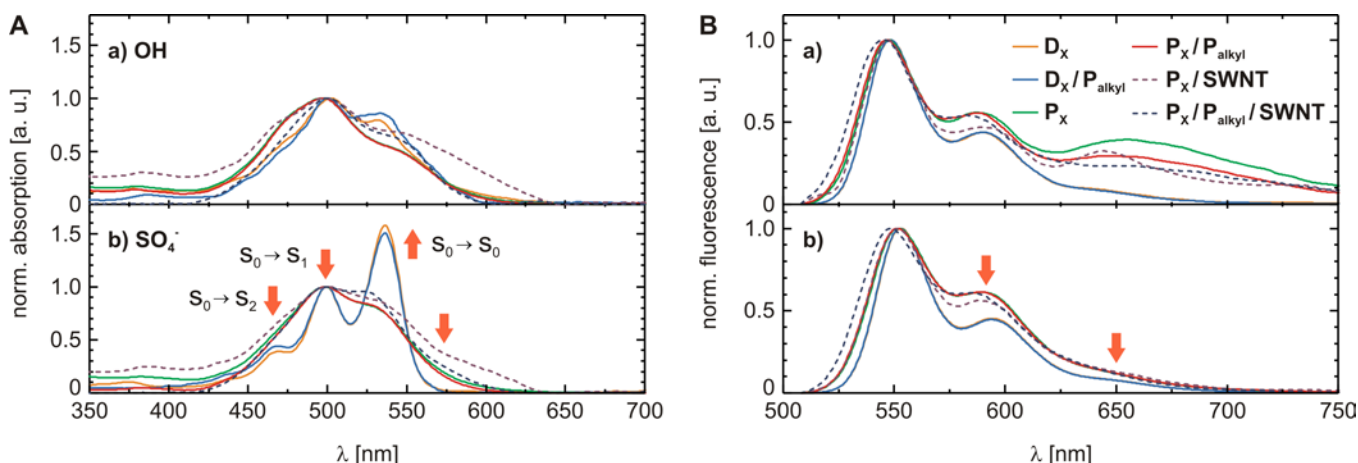


Figure 1. Normalized A) absorption and B) emission spectra of indicated compounds including the free dyes D_X , polymers P_X , and SWNT complexes $P_X / SWNT$ ($c_{P_X} = 0.12 \mu\text{M}$, $c_{SWNT} = 0.01 \text{ g L}^{-1}$, $X = \text{OH}$ or SO_4^-) in mixtures with native polymer P_{alkyl} ($c_{P_{\text{alkyl}}} = 13 \mu\text{M}$) at a dye concentration of $1 \mu\text{M}$ in water at 20°C , see legend in panel B. Absorption spectra were normalized to the $S_0 \rightarrow S_1$ transition; fluorescence spectra on the peak maximum. Arrows indicate the spectroscopic changes from aggregated towards more monomeric PBI species. The molecular electronic transitions belonging to the major absorption bands are denoted next to the arrows. Sulfated species are less aggregated than their hydroxylated analogs due to an additional electrostatic shielding of the dyes.

effect of noncharged versus charged dendritic shielding, the optical properties of hydroxylated and sulfated species were compared. It was found that noncharged hydroxylated species aggregate more strongly than charged sulfated species as shown in Figure 1A. The entire series of hydroxylated compounds displays an absorption pattern arising from strongly aggregated PBIs with low molar absorption coefficients between $12\,500$ and $25\,200 \text{ M}^{-1} \text{ cm}^{-1}$ and inverse peak ratios ≤ 0.86 (Figure 1Aa). The formation of extended aggregates is furthermore expressed by blue-shifted maxima up to 497 nm causing large Stokes shifts between 46 to 51 nm and the appearance of a distinct shoulder at the $S_0 \rightarrow S_2$ transition (Figure 1Aa). In contrast, the sulfated compounds display a less aggregated pattern arising from more monomerized PBIs associated

with significantly higher absorption coefficients between 17 400 and 81 200 $M^{-1} cm^{-1}$ and peak ratios up to 1.58 (Figure 1Ab). The aggregation level increased drastically upon polymer conjugation of the fluorophores as visible in the blue-shifted absorption maxima, reduced peak ratios, and increased Stokes shifts in both systems. Interestingly, the addition of SWNTs supported the monomerization process of PBIs as noticeable in improved A^{0-0}/A^{0-1} ratios rising from 0.56 to 0.70 for hydroxylated and 0.82 to 0.96 for sulfated SWNT complexes. The trend observed in the absorption was also reflected in the emission spectra with a pronounced tailing of the emission band for hydroxylated and a less pronounced tailing for sulfated species mirroring the extent of aggregation (Figure 1B).

The impact of charge and conjugation also becomes visible in the FQYs and brightness depicted in Figure 2A. The sulfated dyes show four to five times higher FQYs than their hydroxylated analogs with a dramatic drop in FQY after polymer conjugation. While the free dyes **D_{OH}** (15%) and **D_{SO₄⁻}** (76%) display moderate to good FQYs, the polymers **P_{OH}** (1.6%) and **P_{SO₄⁻}** (5.9%) show low FQYs as a consequence of dye conjugation that seems to promote the self-quenching of the fluorophores. In contrast to the free dyes, the addition of native polymer **P_{alkyl}** has an advantageous effect on the FQYs of the polymers and SWNT complexes. The difference between neutral versus ionic dendritic shielding is also slightly apparent in the SWNT complexes with higher FQYs for charged alkylated SWNTs (5.1%) than for the analogous neutral alkylated SWNTs (4.3%). According to the trend observed in the FQYs, the brightness increases due to enhanced luminescence properties of polyionic PBIs, which becomes apparent in the change of color from pale pink for **D_{OH}** to bright orange for **D_{SO₄⁻}** as seen in Figure 2B (also see Figure S14).^[17, 79] The difference between the hydroxylated and sulfated polymers **P_x** is less obvious; however, both polymers are able to highly solubilize and

homogeneously distribute SWNTs in aqueous solution as seen by the dark brown color of the polymer-wrapped SWNT complexes $\mathbf{P}_X / \text{SWNT}$.

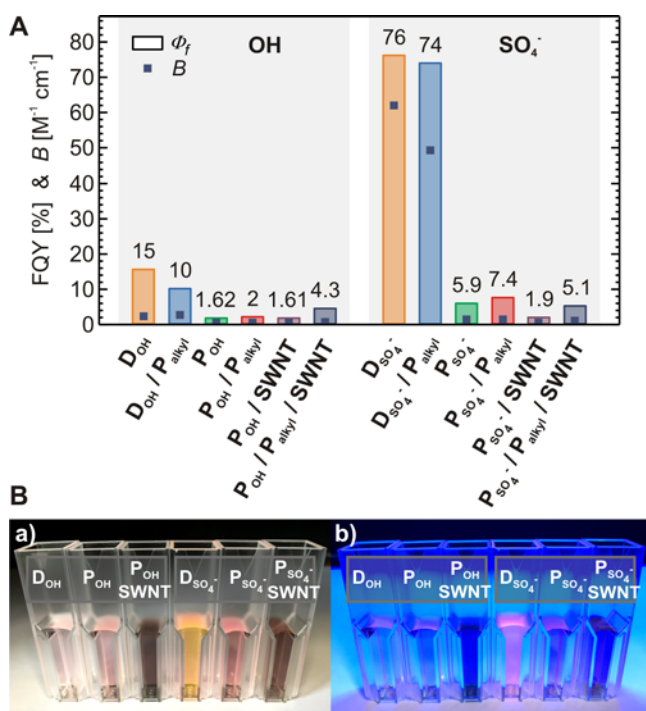


Figure 2. A) FQYs (columns) and brightness (symbols) of indicated compounds at a dye concentration of 1 μM in water at 20 $^{\circ}\text{C}$. B) Hydroxylated and sulfated free dyes \mathbf{D}_X , dye polymers \mathbf{P}_X , and SWNT complexes $\mathbf{P}_X / \text{SWNT}$ ($c_{\mathbf{P}_X} = 0.12 \mu\text{M}$, $c_{\text{SWNT}} = 0.01 \text{ g L}^{-1}$, $X = \text{OH}$ or SO_4^-) in aqueous solution under a) daylight and b) UV light illumination at a dye concentration of 1 μM . The FQYs and aqueous solutions show higher luminescence properties for charged species than for noncharged species.

Summarizing the results, ionic groups onto dendronized PBIs are beneficial for sufficiently shielding the π -faces of aromatic PBIs in water, which was confirmed by higher FQYs of charged species over their neutral counterparts. Although the optical properties decreased drastically after polymer conjugation, comparable FQYs of the SWNT complexes (4.3% and 5.1%) to commercially available fluorescent dyes such as cy3^[12] or bodipy^[14] (both 4%) confirmed the suitability of our complexes for the planned biological studies.

2.3 Dispersibility of the SWNT Complexes

To exploit the biological potential of our SWNT complexes, we had to ensure that the SWNTs are well isolated and the PBI emission is preserved. Photoluminescence excitation (PLE) measurements were conducted to observe the dispersion of the SWNTs and the influence of the PBIs on the tubes and vice versa.^[82-83] We monitored the emission of the SWNTs to estimate the polymers' solubilization ability and any potential dye-tube interactions as depicted in the 2D PLE map of the sulfated complex $\mathbf{Pso}_4^- / \mathbf{P}_{\text{alkyl}} / \mathbf{SWNT}$ in Figure 4Aa (for the hydroxylated analog see Figure S16, ESI). The map shows that we were able to identify up to 12 different SWNT chiralities after debundling,^[82-85] which proves the successful solubilization of the tubes. The yellow highlighted region in the PLE map corresponds to the absorption region of the sulfated dye polymer \mathbf{Pso}_4 , shown on the left side of the panel in Figure 4Ab. Indirect emission of the SWNTs mediated by the PBIs would have occurred in this region.^[49, 86] For the neutral and charged PBI-SWNT complexes no indirect excitation of the tubes through the dye was observed, which allowed the use of our functionalized SWNTs as fluorescent labels.

To guarantee the use of our multifunctional platform as a bioimaging agent, a strong fluorescence signal of the PBI labels is required. We monitored the emission of the PBIs to exclude quenching due to energy or charge transfer processes with the SWNTs. After the SWNT functionalization with the dye polymer, we observed a drop in the emission intensity of the PBI of approximately 75% as seen in Figure 4B. The quenching is an indication for the close proximity of the perylene to the tubes as reported by Ernst *et al.*, who observed quenching effects in the order of 10^4 .^[49] The quenching observed in our complex system is weak indicating that the polymer wrapping results in a greater dye to tube separation. When further promoting the debundling of the SWNTs by adding the native polymer $\mathbf{P}_{\text{alkyl}}$, we observed an increase of the PBI emission, which gets restored up to 50% of its initial intensity. Thus, the native polymer further covers the tubes and reduces undesired dye-tube interactions. After verifying

that the PBI emission is preserved after formation of the polymer-SWNT complex, we performed cytotoxicity and cellular uptake *in vitro* studies to test their validity for bioimaging purposes.

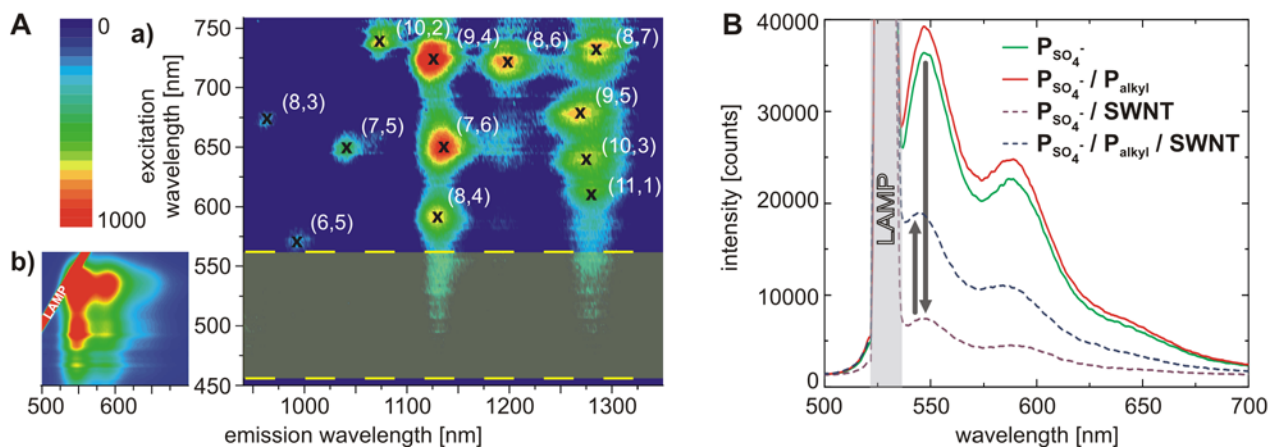


Figure 4. A a) The 2D-PLS map of debundled complexes $\text{P}_{\text{SO}_4^-} / \text{P}_{\text{alkyl}} / \text{SWNT}$ shows no energy transfer in the expected excitation window between 460 to 560 nm. A b) 2D-PLS map of sulfated dye polymer $\text{P}_{\text{SO}_4^-}$. B) PBI emission spectra of indicated compounds with sulfated dye polymer $\text{P}_{\text{SO}_4^-}$ at an excitation wavelength of 530 nm. The functionalization of dye polymer $\text{P}_{\text{SO}_4^-}$ onto the SWNTs leads to a 75% decrease of the PBI emission intensity. Later addition of native polymer P_{alkyl} recovers the emission to 50% of its original intensity. The maps and spectra of the dye polymer ($c_{\text{dye}} = 10 \mu\text{M}$, corresponds to $c_{\text{P}_{\text{SO}_4^-}} = 1.18 \mu\text{M}$), native polymer ($c_{\text{P}_{\text{alkyl}}} = 130 \mu\text{M}$), and SWNTs ($c_{\text{SWNT}} = 0.1 \text{ g L}^{-1}$) were measured at indicated concentrations in aqueous solution at 20 °C.

2.4 Biological Evaluation

2.4.1. Toxicity Study

Despite the expansion of potential biomedical applications for SWNTs, their usage is still limited due to poor biocompatibility and toxic side effects, caused by the high aspect ratio (length to side proportion) and surface area of the SWNT scaffold.^[87-89] The solubilization with commercial surfactants such as sodium dodecyl sulfate (SDS) or Triton X-100 further strongly compromises the already low cytocompatibility of SWNTs.^[90-91] Typically, large amounts of surfactant are needed to sufficiently solubilize the SWNTs due to the relatively high CMC of these amphiphiles. The excess of surfactant might lyse the lipid cell membrane and denature cellular proteins causing cell death.^[91] We hypothesized that a surfactant-free functionalization

by polymer wrapping would cover the SWNT surface and therefore reduce their toxicity.^[59-62] To investigate whether polymer wrapping promotes the cytocompatibility of our SWNT complexes, we performed a toxicity study with the HeLa cell line. The viability of HeLa cells treated with the free dyes, polymers, SWNT complexes, and pristine SWNTs was monitored after an incubation time of 24 h as depicted in the different sections of Figure 5A. The results in the sections *OH*, *SO₄⁻*, and *Native* demonstrate a high cell viability of the free dyes, polymers, and SWNT complexes with viability rates around 100% proving no cytotoxic effects at the tested concentration. The advantageous application of our polymers towards commercially available surfactants is demonstrated in the *Surfactant* section. As comparative surfactants, non-ionic polyether block copolymer Pluronic and ionic alkyl sulfate SDS were chosen. While our polymer-solubilized SWNTs were able to increase the cell viability of pristine SWNTs from 66% to $\geq 98\%$, surfactant-solubilized SWNTs decreased their viability to $\leq 20\%$. The cellular degradation triggered by surfactant solubilization of the SWNTs can additionally be seen in Figure 5B (also see Figure S19, ESI). While cells treated with **P_{alkyl}**-solubilized SWNTs show good viability, cells treated with SDS-solubilized SWNTs have a high rate of mortality even up to the extinction of the entire cell population.

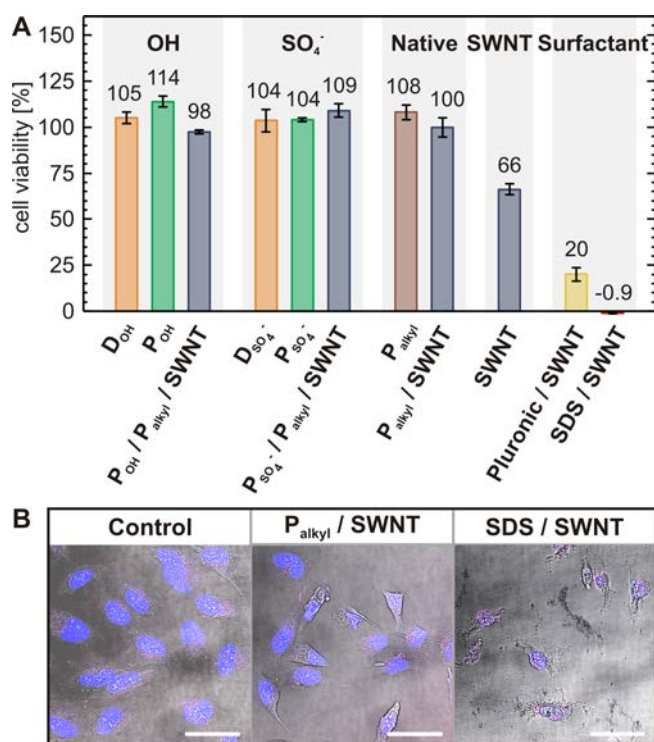


Figure 5. A) Cytotoxicity study of HeLa cells incubated with free dyes D_X , dye polymers P_X ($c_{dye} = 1 \mu M$, corresponds to $c_{P_X} = 0.12 \mu M$, $X = OH$ or SO_4^-), native polymer P_{alkyl} ($c = 0.13 \mu M$), and SWNT complexes ($c_{SWNT} = 0.01 g L^{-1}$). For comparison, HeLa cells were further incubated with pristine SWNTs or surfactant-solubilized SWNTs ($c_{surf.} = 1 wt. \%$). The values obtained were normalized to the nontreated cell population as control. B) Live-cell microscopy images of HeLa cells treated with P_{alkyl} -solubilized SWNTs and surfactant-solubilized SWNTs. The control represents the untreated cell population. Cell nuclei are shown in blue. Scale bar: $50 \mu m$. The study shows good cell viability with our polymer-wrapped SWNT complexes and low viability up to cell death with surfactant-solubilized SWNTs.

2.4.2. Microscopy and Flow Cytometry

To assess the uptake behavior and staining efficiency of the polymer-SWNT complexes, *in vitro* studies on human epithelial HeLa cells were performed. The cellular uptake of the free dyes, polymers, and SWNT complexes was qualitatively monitored by live-cell confocal microscopy and quantitatively analyzed by flow cytometry as shown in Figure 6 (see Figure S17 and S18 for the entire series of test compounds). After an incubation time of 4 hours, the neutral or charged free dyes D_X ($X = OH$ or SO_4^-) could not be detected inside the cells. In contrast, the dye-conjugated polymers P_X and complexes $P_X / P_{alkyl} / SWNT$ showed an active uptake as seen by the intracellular fluorescence signals of the PBI dye. Hence, a covalent binding between the dye and the polymer backbone is required for the cellular uptake of the

dyes. This observation was further proven by the fact that neither the free dyes **D_x** nor the free dyes mixed with native polymer **D_x / P_{alkyl}** showed an internal signal inside the cells (see Figure S17 and S18). PEG-based architectures feature a high biocompatibility and rapid cellular uptake;^[92-93] covalent PEGylation of multi-walled carbon nanotubes (MWNT) proved to be a useful tool for improving the dispersion ability and biocompatibility of the tubes.^[94] Given the facts, it can be assumed that the uptake of the dyes was supported by the conjugation to the PEGylated polymer. Therefore, polymer conjugation is essential for the performed imaging studies as it efficiently promotes the cellular uptake of the PBIs and prevents intermolecular π - π interactions of the dyes among each other or with the SWNT scaffold.

The dye-conjugated polymers **P_x** and complexes **P_x / P_{alkyl} / SWNT** show a vesicular uptake pattern for the hydroxylated and sulfated compounds after internalization into the cytoplasm of the cell (Figure 6A). The vesicular staining pattern presumably stems from cytoplasmic inclusions of the polymers or complexes inside lysosomes and endosomes internalized by endocytosis. As expected, the sulfated polymers and complexes show more intense intracellular fluorescence signals compared to their hydroxylated analogs. These findings are in line with the results gained in a recent study analyzing the uptake and cellular fate of highly anionic sulfated nanoparticles in comparison to neutral hydroxylated particles.^[38] The study showed, that sulfated moieties increase the cellular uptake rate of nanoparticles via endocytotic pathways in particular phagocytosis whereas hydroxylated particles are less or even not taken up by the cells due to their neutral charge, related protein-resistant properties, and weak nonspecific interactions with biological components. Sulfated compounds in contrast are able to interact with scavenger receptors^[95] on the cells, that can mediate the uptake of polyanionic ligands such as dextran sulfate, which leads to an improved uptake of sulfated over hydroxylated compounds. In addition to the improved uptake, the brighter signals stem from a

reinforced sterical shielding of the ionic sulfate groups, which further prevent dye-dye self-quenching.

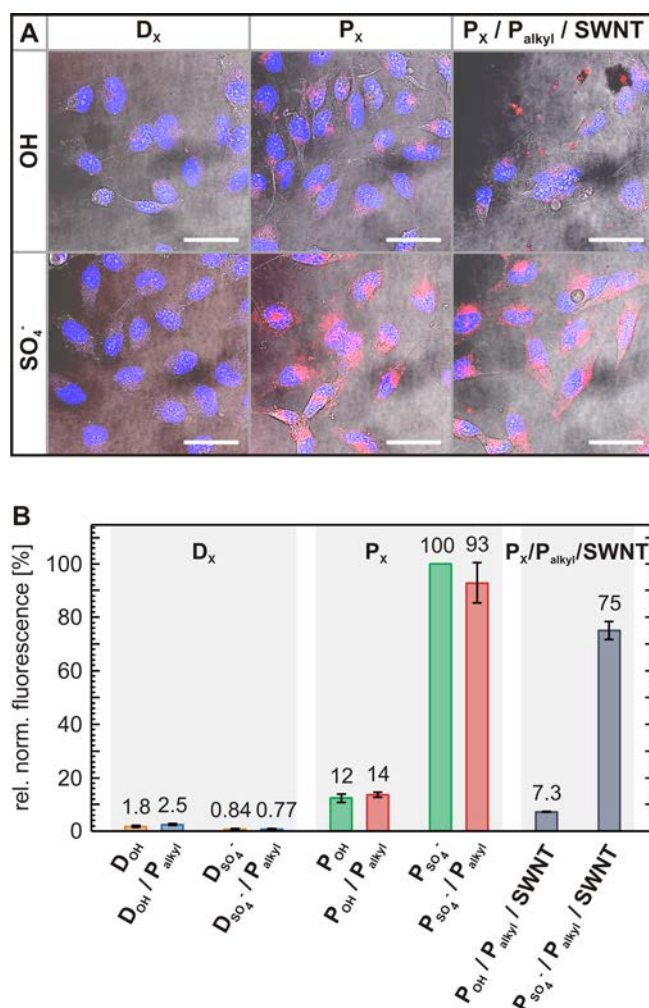


Figure 6. *In vitro* cellular uptake studies of hydroxylated and sulfated free dyes **D_x**, dye polymers **P_x** ($c_{\text{dye}} = 1 \mu\text{M}$, corresponds to $c_{\text{P}_X} = 0.12 \mu\text{M}$), and complexes **P_x / P_{alkyl} / SWNT** ($c_{\text{SWNT}} = 0.01 \text{ g L}^{-1}$, $X = \text{OH}$ or SO_4^-). A) Live-cell microscopy images of HeLa cells treated with indicated PBI-based compounds (red) after 4 h of incubation. Cell nuclei are shown in blue. Scale bar: 50 μm . B) Flow cytometry analysis of HeLa cells treated with indicated compounds. The bars represent the mean fluorescence intensities of three independent measurements \pm standard error of the mean. The fluorescence intensities are relative to the normalized intensity of **P_{SO₄⁻}**. The results prove an improved uptake behavior and staining efficiency of sulfated over hydroxylated polymers and complexes.

Flow cytometry analysis confirmed the trend seen in the microscopy study with low intracellular fluorescence intensities for the free dyes **D_x** and higher intensities for the polymers **P_x** and complexes (Figure 6B). It is noteworthy that while hydroxylated species display higher

fluorescence intensities with the addition of $\mathbf{P}_{\text{alkyl}}$, their sulfated counterparts showed a reversed effect. Presumably, $\mathbf{P}_{\text{alkyl}}$ suppresses the Coulombic repulsion forces of the sulfate groups thereby diminishing their effect. However, also in flow cytometry the different uptake behavior and staining efficiency of SO_4^- vs. OH is apparent with fluorescence intensities of 75% for sulfated complex and 7.3% for its hydroxylated analog in relation to $\mathbf{P}_{\text{SO}_4^-}$ (normalized to 100%).

2.4.3. Raman Imaging

As the polymer wrapping ensures a strong immobilization of the PBIs on the SWNTs, we assumed that an intracellular signal of the dye polymer simultaneously indicates the cellular uptake of the SWNTs. The observation of red fluorescence signals around small SWNT aggregates visible in the zoomed microscopy images indirectly confirmed the uptake of the entire complex system (see overlay channel in Figure S20). However, the size of single pristine SWNTs is below the resolution limit of the optical microscope. Additionally, the intrinsic fluorescence of debundled SWNTs above 1000 nm is out of the detection range of the used confocal microscope (400 to 800 nm). Thus, confocal microscopy solely ensured the uptake of the PBI-moieties as we monitor the PBI fluorescence. To affirm the cellular uptake of the entire multifunctional polymer-SWNT complex, we performed Raman spectroscopy. It was previously reported that the cellular uptake of functionalized graphene sheets could be monitored via Raman microscopy.^[38]

We employed Raman spectroscopy combined with PL measurements to verify the cellular uptake of the PBI-covered SWNTs. Several cells were incubated with the sulfated polymer-SWNT complex as our brightest complex and scanned with an optical microscope. Figure 7A depicts a set of cells with a 10-times amplification. The red frame highlights the area in which the PL and Raman signals of the selected cell were recorded. For the excitation of the PBI-

polymer, the 532 nm laser line was used to match the PBI $S_0 \rightarrow S_0$ electronic transition. At this excitation, two emission bands at 550 nm and 592 nm dominate the optical signal. In Figure 7B the intensity of the 592 nm PBI emission band is shown as a function of the spatial position. A strong signal from the area inside the cell could be detected indicating the successful uptake of the sulfated dye polymer into the cell.

To ensure whether the polymer is still wrapped around the SWNTs after the cellular internalization, Raman spectroscopy of the SWNT complexes was performed using the laser excitation line at 638 nm. The Raman spectra revealed the radial breathing mode of the SWNTs, the G and the 2D band (see Figure S21). In Figure 7C, the spatial distribution of the SWNTs' Raman G band inside and outside the cell is depicted. The high image contrast confirms the successful uptake of the functionalized SWNTs inside the living cell. Both the spatially resolved PL signal of the PBI and the Raman signal of the SWNTs strongly resemble the shape of the cell acquired in the microscope image. The overlapping of the PBI-polymers' PL and the SWNTs' Raman signals indicate that the PBI-SWNT complex remains unperturbed after the cellular uptake. Despite the low FQY^[5-7] of SWNTs, we were able to demonstrate the uptake of the functionalized SWNT complexes by directly monitoring the PL signal of the (8,3) tube species. By exciting the SWNTs at 650 nm while monitoring their emission at 980 nm ($E_{22} \rightarrow E_{11}$), we further established the spatially resolved map of the tube emission intensity depicted in Figure 7D. The spatial distribution of the nanotube emission strongly overlaps with the distribution obtained from the PBI emission in Figure 7B, which confirms that we were able to detect the complexes in the 1st and 2nd transparency window of tissue. These results prove three major findings: i) the successful cellular uptake of the SWNT complex, ii) the stability of the platform by the strong polymer wrapping of the SWNTs, and iii) the direct monitoring of the cellular uptake through several independent system parameters. These results demonstrate the solidity and versatility of our multifunctional SWNT complex.

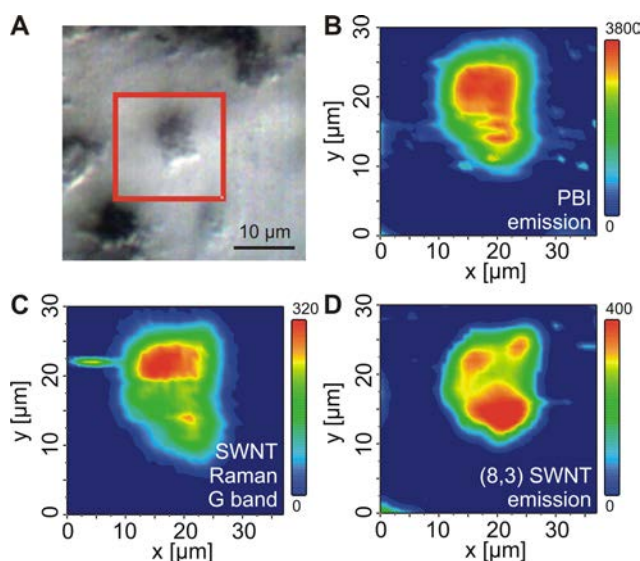


Figure 7. A) Optical image of HeLa cells incubated with sulfated complex $\text{Pso}_4^- / \text{Palkyl} / \text{SWNT}$. The red frame shows the area in which PL and Raman measurements were conducted. B) Spatial PL map of the PBI' emission excited at 532 nm. C) Spatial distribution of the SWNTs' Raman G band excited at 638 nm. D) Spatial PL map of the (8,3) SWNTs' emission excited at 650 nm. The intracellular emission signal of the SWNTs strongly resembles the shape of the investigated HeLa cell, thus, indicating a successful internalization of the entire polymer-SWNT complex into the cell.

To summarize, the prepared SWNT complexes were well tolerated by the utilized cell line without cytotoxic side effects. The cellular uptake of the entire polymer-SWNT complex was proven by the PBI and SWNT emission in combination with the SWNT Raman signal. To achieve a bright fluorescence signal upon cellular staining, sulfated SWNT complexes were required due to better uptake properties and staining efficiencies.

3. Summary and Conclusion

We developed a charge neutral and charged version of a multifunctional polymer-SWNT complex and probed their performance as bioimaging agents. The rationally designed complex consists of dendronized PBIs as fluorescent labels, long alkyl chains as hydrophobic units, a polymer backbone as solubilizing and shielding moiety, and SWNTs as general immobilization platform. The optical characterization of the complexes revealed moderate FQYs of 4.3% for the hydroxylated and 5.1% for the sulfated SWNT complexes. None of the hybrid systems

showed energy transfer processes suggesting a preserved PBI luminescence after complex formation. The biological suitability of the complexes was analyzed by toxicity and uptake *in vitro* studies on HeLa cells. The cytotoxicity study displayed the superior compatibility of the polymer-wrapped SWNTs compared to pristine or surfactant-solubilized SWNTs; the cellular uptake study revealed the internalization of the entire intact polymer-SWNT complex via the PBI and SWNT emission. To achieve a bright fluorescent signal inside the cells, the introduction of charged groups onto the dendronized PBIs is required for an improved receptor-mediated cellular uptake behavior and intrinsic aggregation suppression of the complexes.

We demonstrated that the functionalization of SWNTs with PBI-conjugated polymers results in water-soluble, fluorescent, and debundled SWNT complexes suitable for bioimaging studies. Our supramolecular complex allowed for the direct imaging of the SWNTs' cellular uptake and drastically improved their cytocompatibility. The combination of PBI fluorophores and intrinsically fluorescent SWNTs allowed the intracellular detection of the complexes in the 1st and 2nd optical transparency window of tissue. The development of such a dual imaging system is non-trivial since transfer processes between the fluorophores and SWNTs can cause the luminescence quenching of the dyes. These results render the sulfated multifunctional SWNT complexes as potent candidates in fluorescent bioimaging for a broad readout in two optical windows. The versatile modification routine for the formation of SWNT complexes with multipurpose functionalities may furthermore be of great benefit for sophisticated biomedical applications in the future.

Supporting Information

Supporting Information including experimental details of the synthesis, photophysical characterization, and biological evaluation is available from the authors.

Acknowledgements

‡ Author 1 and Author 2 contributed equally to this work.

The authors gratefully acknowledge Deutsche Forschungsgemeinschaft (SFB 658) and Focus Area NanoScale of Freie Universität Berlin for their financial support. The authors thank Elisa Quaas for her assistance in the biological experiments, Katharina Goltsche and Marleen Selent for their technical assistance in the dendron synthesis and HPLC, and Cathleen Schlesener for GPC measurements. Furthermore, we thank Sabrina Juergensen for her help with the PL measurements.

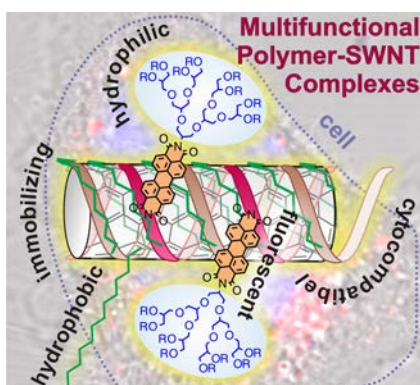
TOC

It's the mixture that counts: Dyes + Polymers + SWNTs = multifunctional Complexes! The combination of bright fluorophores, cytocompatible polymers, and SWNTs as basic immobilization platform leads to highly fluorescent polymer-SWNT complexes for bioimaging applications. The multifunctional system enables the direct imaging of the SWNTs' cellular uptake in two optical transparency windows and strongly improves their cytocompatibility.

Bioimaging

Katharina Huth,[‡] Mareen Gläske,[‡] Katharina Achazi, Georgy Gordeev, Shiv Kumar, Raúl Arenal, Sunil K. Sharma, Mohsen Adeli, Antonio Setaro,* Stephanie Reich, and Rainer Haag*
Synthesis and Characterization of Fluorescent Polymer - Single-Walled Carbon Nanotube Complexes with Noncharged and Charged Dendronized Perylene Bisimides for Bioimaging Studies

ToC figure



References

- [1] E. Heister, V. Neves, C. Tîlmaciu, K. Lipert, V. S. Beltrán, H. M. Coley, S. R. P. Silva, J. McFadden, *Carbon* **2009**, *47*, 2152-2160.
- [2] M. Ferrari, *Nat. Rev. Cancer* **2005**, *5*, 161-171.
- [3] S. Beg, M. Rizwan, A. M. Sheikh, M. S. Hasnain, K. Anwer, K. Kohli, *J. Pharm. Pharmacol.* **2011**, *63*, 141-163.
- [4] A. M. Smith, M. C. Mancini, S. Nie, *Nat. Nanotechnol.* **2009**, *4*, 710-711.
- [5] D. A. Tsyboulski, J.-D. R. Rocha, S. M. Bachilo, L. Cagnet, R. B. Weisman, *Nano Lett.* **2007**, *7*, 3080-3085.
- [6] A. Hagen, M. Steiner, M. B. Raschke, C. Lienau, T. Hertel, H. Qian, A. J. Meixner, A. Hartschuh, *Phys. Rev. Lett.* **2005**, *95*, 197401.
- [7] J. Lefebvre, D. G. Austing, J. Bond, P. Finnie, *Nano Lett.* **2006**, *6*, 1603-1608.
- [8] H. Gong, R. Peng, Z. Liu, *Adv. Drug Del. Rev.* **2013**, *65*, 1951-1963.
- [9] K. Welsher, Z. Liu, S. P. Sherlock, J. T. Robinson, Z. Chen, D. Daranciang, H. Dai, *Nat. Nanotechnol.* **2009**, *4*, 773-780.
- [10] R. Lehner, X. Wang, S. Marsch, P. Hunziker, *Nanomed. Nanotechnol. Biol. Med.*, *9*, 742-757.
- [11] M. Glaeske, A. Setaro, *Nano Res.* **2013**, *6*, 593-601.
- [12] M. Cooper, A. Ebner, M. Briggs, M. Burrows, N. Gardner, R. Richardson, R. West, *J. Fluoresc.* **2004**, *14*, 145-150.
- [13] Y. Li, Y. Bai, N. Zheng, Y. Liu, G. A. Vincil, B. J. Pedretti, J. Cheng, S. C. Zimmerman, *Chem. Commun.* **2016**, *52*, 3781-3784.
- [14] S. Zhu, J. Zhang, G. Vegesna, F.-T. Luo, S. A. Green, H. Liu, *Org. Lett.* **2011**, *13*, 438-441.

- [15] T. Weil, T. Vosch, J. Hofkens, K. Peneva, K. Müllen, *Angew. Chem. Int. Ed.* **2010**, *49*, 9068-9093.
- [16] M. Sun, K. Müllen, M. Yin, *Chem. Soc. Rev.* **2016**, *45*, 1513-1528.
- [17] K. Huth, T. Heek, K. Achazi, C. Kühne, L. H. Urner, K. Pagel, J. Dervedde, R. Haag, *Chem. Eur. J.* **2017**, *23*, 4849-4862.
- [18] K. Peneva, G. Mihov, F. Nolde, S. Rocha, J.-i. Hotta, K. Braeckmans, J. Hofkens, H. Uji-i, A. Herrmann, K. Müllen, *Angew. Chem. Int. Ed.* **2008**, *47*, 3372-3375.
- [19] J. Qu, C. Kohl, M. Pottek, K. Müllen, *Angew. Chem. Int. Ed.* **2004**, *43*, 1528-1531.
- [20] K. Peneva, G. Mihov, A. Herrmann, N. Zarrabi, M. Börsch, T. M. Duncan, K. Müllen, *J. Am. Chem. Soc.* **2008**, *130*, 5398-5399.
- [21] S. K. Yang, X. Shi, S. Park, S. Doganay, T. Ha, S. C. Zimmerman, *J. Am. Chem. Soc.* **2011**, *133*, 9964-9967.
- [22] T. Heek, J. Nikolaus, R. Schwarzer, C. Fasting, P. Welker, K. Licha, A. Herrmann, R. Haag, *Bioconjugate Chem.* **2013**, *24*, 153-158.
- [23] C. Jung, B. K. Müller, D. C. Lamb, F. Nolde, K. Müllen, C. Bräuchle, *J. Am. Chem. Soc.* **2006**, *128*, 5283-5291.
- [24] T. Heek, C. Kühne, H. Depner, K. Achazi, J. Dervedde, R. Haag, *Bioconjugate Chem.* **2016**, *27*, 727-736.
- [25] E. Fron, G. Schweitzer, P. Osswald, F. Würthner, P. Marsal, D. Beljonne, K. Müllen, F. C. De Schryver, M. Van der Auweraer, *Photochem. Photobiol. Sci.* **2008**, *7*, 1509-1521.
- [26] R. Boerner, D. Kowerko, S. Krause, C. von Borczyskowski, C. G. Huebner, *J. Chem. Phys.* **2012**, *137*, 164202/164201-164202/164211.
- [27] D. Aigner, R. I. Dmitriev, S. M. Borisov, D. B. Papkovsky, I. Klimant, *J. Mater. Chem. B* **2014**, *2*, 6792-6801.
- [28] W. E. Ford, P. V. Kamat, *J. Phys. Chem.* **1987**, *91*, 6373-6380.

- [29] M. J. Farooqi, M. A. Penick, J. Burch, G. R. Negrete, L. Brancalione, *Spectrochim. Acta, Part A* **2016**, *153*, 124-131.
- [30] D. Li, Z. Tian, J. Zhang, *Res. Chem. Intermed.* **2013**, *39*, 1665-1671.
- [31] M. Y. Berezin, S. Achilefu, *Chem. Rev.* **2010**, *110*, 2641-2684.
- [32] Y. Li, K. Huth, E. S. Garcia, B. J. Pedretti, Y. Bai, G. A. Vincil, R. Haag, S. C. Zimmerman, *Polym. Chem.* **2018**, *9*, 2040-2047.
- [33] C. Kohl, T. Weil, J. Qu, K. Müllen, *Chem. Eur. J.* **2004**, *10*, 5297-5310.
- [34] Q. Zhou, Y. Hou, L. Zhang, J. Wang, Y. Qiao, S. Guo, L. Fan, T. Yang, L. Zhu, H. Wu, *Theranostics* **2017**, *7*, 1806-1819.
- [35] M. Yin, J. Shen, G. O. Pflugfelder, K. Müllen, *J. Am. Chem. Soc.* **2008**, *130*, 7806-7807.
- [36] M. Yin, J. Shen, R. Gropeanu, G. O. Pflugfelder, T. Weil, K. Müllen, *Small* **2008**, *4*, 894-898.
- [37] M. Yin, C. R. W. Kuhlmann, K. Sorokina, C. Li, G. Mihov, E. Pietrowski, K. Koynov, M. Klapper, H. J. Luhmann, K. Müllen, T. Weil, *Biomacromolecules* **2008**, *9*, 1381-1389.
- [38] Z. Tu, K. Achazi, A. Schulz, R. Mülhaupt, S. Thierbach, E. Rühl, M. Adeli, R. Haag, *Adv. Funct. Mater.* **2017**, *27*, 1701837-n/a.
- [39] C. Backes, C. D. Schmidt, F. Hauke, C. Böttcher, A. Hirsch, *J. Am. Chem. Soc.* **2009**, *131*, 2172-2184.
- [40] C. Backes, C. D. Schmidt, F. Hauke, A. Hirsch, *Chem. Asian J.* **2011**, *6*, 438-444.
- [41] C. Ehli, C. Oelsner, D. M. Guldi, A. Mateo-Alonso, M. Prato, C. Schmidt, C. Backes, F. Hauke, A. Hirsch, *Nat. Chem.* **2009**, *1*, 243-249.
- [42] C. Backes, F. Hauke, C. D. Schmidt, A. Hirsch, *Chem. Commun.* **2009**, 2643-2645.
- [43] C. Backes, E. Karabudak, C. D. Schmidt, F. Hauke, A. Hirsch, W. Wohlleben, *Chem. Eur. J.* **2010**, *16*, 13176-13184.

- [44] C. Backes, U. Mundloch, C. D. Schmidt, J. N. Coleman, W. Wohlleben, F. Hauke, A. Hirsch, *Chem. Eur. J.* **2010**, *16*, 13185-13192.
- [45] C. Oelsner, C. Schmidt, F. Hauke, M. Prato, A. Hirsch, D. M. Guldi, *J. Am. Chem. Soc.* **2011**, *133*, 4580-4586.
- [46] F. Ernst, T. Heek, A. Setaro, R. Haag, S. Reich, *J. Phys. Chem. C* **2013**, *117*, 1157-1162.
- [47] F. Ernst, Z. Gao, R. Arenal, T. Heek, A. Setaro, R. Fernandez-Pacheco, R. Haag, L. Cognet, S. Reich, *J. Phys. Chem. C* **2017**, *121*, 18887-18891.
- [48] F. Ernst, T. Heek, R. Haag, S. Reich, A. Setaro, *Phys. Status Solidi B* **2012**, *249*, 2465-2468.
- [49] F. Ernst, T. Heek, A. Setaro, R. Haag, S. Reich, *Adv. Funct. Mater.* **2012**, *22*, 3921-3926.
- [50] A. Nish, J.-Y. Hwang, J. Doig, R. J. Nicholas, *Nat. Nanotechnol.* **2007**, *2*, 640.
- [51] P. Deria, C. D. Von Bargen, J.-H. Olivier, A. S. Kumbhar, J. G. Saven, M. J. Therien, *J. Am. Chem. Soc.* **2013**, *135*, 16220-16234.
- [52] J. Budhathoki-Uprety, R. E. Langenbacher, P. V. Jena, D. Roxbury, D. A. Heller, *ACS Nano* **2017**, *11*, 3875-3882.
- [53] R. Soleyman, S. Hirbod, M. Adeli, *Biomater. Sci.* **2015**, *3*, 695-711.
- [54] M. Adeli, S. Beyranvand, R. Kabiri, *Polym. Chem.* **2013**, *4*, 669-674.
- [55] M. J. O'Connell, P. Boul, L. M. Ericson, C. Huffman, Y. Wang, E. Haroz, C. Kuper, J. Tour, K. D. Ausman, R. E. Smalley, *Chem. Phys. Lett.* **2001**, *342*, 265-271.
- [56] A. Liu, T. Watanabe, I. Honma, J. Wang, H. Zhou, *Biosens. Bioelectron.* **2006**, *22*, 694-699.
- [57] S. Kruss, D. P. Salem, L. Vukovic, B. Lima, E. Vander Ende, E. S. Boyden, M. S. Strano, *Proc. Natl. Acad. Sci. U. S. A.* **2017**, *114*, 1789-1794.
- [58] S. Kruss, A. J. Hilmer, J. Zhang, N. F. Reuel, B. Mu, M. S. Strano, *Adv. Drug Delivery Rev.* **2013**, *65*, 1933-1950.

- [59] J. T. Robinson, G. Hong, Y. Liang, B. Zhang, O. K. Yaghi, H. Dai, *J. Am. Chem. Soc.* **2012**, *134*, 10664-10669.
- [60] P. Petrov, G. Georgiev, D. Momekova, G. Momekov, C. B. Tsvetanov, *Polymer* **2010**, *51*, 2465-2471.
- [61] R. M. Sankar, K. M. S. Meera, D. Samanta, A. Murali, P. Jithendra, A. Baran Mandal, S. N. Jaisankar, *RSC Adv.* **2012**, *2*, 12424-12430.
- [62] I. Armentano, M. Dottori, E. Fortunati, S. Mattioli, J. M. Kenny, *Polym. Degrad. Stab.* **2010**, *95*, 2126-2146.
- [63] J. Zhang, M. P. Landry, P. W. Barone, J.-H. Kim, S. Lin, Z. W. Ulissi, D. Lin, B. Mu, A. A. Boghossian, A. J. Hilmer, A. Rwei, A. C. Hinckley, S. Kruss, M. A. Shandell, N. Nair, S. Blake, F. Sen, S. Sen, R. G. Croy, D. Li, K. Yum, J.-H. Ahn, H. Jin, D. A. Heller, J. M. Essigmann, D. Blankschtein, M. S. Strano, *Nat. Nanotechnol.* **2013**, *8*, 959-968.
- [64] N. B. Saleh, D. Das, J. Plazas-Tuttle, D. Yang, J. T. Del Bonis-O'Donnell, M. P. Landry, *NanoImpact* **2017**, *6*, 90-98.
- [65] M. P. Landry, H. Ando, A. Y. Chen, J. Cao, V. I. Kottadiel, L. Chio, D. Yang, J. Dong, T. K. Lu, M. S. Strano, *Nat. Nanotechnol.* **2017**, *12*, 368.
- [66] S. Kruss, M. P. Landry, E. Vander Ende, B. M. A. Lima, N. F. Reuel, J. Zhang, J. Nelson, B. Mu, A. Hilmer, M. Strano, *J. Am. Chem. Soc.* **2014**, *136*, 713-724.
- [67] Z. Chen, A. Lohr, C. R. Saha-Möller, F. Würthner, *Chem. Soc. Rev.* **2009**, *38*, 564-584.
- [68] M. Weinhart, D. Groeger, S. Enders, S. B. Riese, J. Dervedde, R. K. Kainthan, D. E. Brooks, R. Haag, *Macromol. Biosci.* **2011**, *11*, 1088-1098.
- [69] S. Kumar, K. Achazi, C. Böttcher, K. Licha, R. Haag, S. K. Sharma, *Eur. Polym. J.* **2015**, *69*, 416-428.

- [70] V. Hong, S. I. Presolski, C. Ma, M. G. Finn, *Angew. Chem. Int. Ed.* **2009**, *48*, 9879-9883.
- [71] K. Petkau-Milroy, L. Brunsveld, *Eur. J. Org. Chem.* **2013**, *2013*, 3470-3476.
- [72] C. Lim, T. Sim, N. H. Hoang, C. E. Jung, E. S. Lee, Y. S. Youn, K. T. Oh, *Int. J. Nanomed.* **2017**, *12*, 6185-6196.
- [73] Y. Skhiri, P. Gruner, B. Semin, Q. Brosseau, D. Pekin, L. Mazutis, V. Goust, F. Kleinschmidt, A. El Harrak, J. B. Hutchison, E. Mayot, J.-F. Bartolo, A. D. Griffiths, V. Taly, J.-C. Baret, *Soft Matter* **2012**, *8*, 10618-10627.
- [74] Z. Chen, V. Stepanenko, V. Dehm, P. Prins, L. D. A. Siebbeles, J. Seibt, P. Marquetand, V. Engel, F. Würthner, *Chem. Eur. J.* **2007**, *13*, 436-449.
- [75] J. M. Lim, P. Kim, M.-C. Yoon, J. Sung, V. Dehm, Z. Chen, F. Würthner, D. Kim, *Chem. Sci.* **2013**, *4*, 388-397.
- [76] Z. Chen, U. Baumeister, C. Tschierske, F. Würthner, *Chem. Eur. J.* **2007**, *13*, 450-465.
- [77] F. Würthner, C. Thalacker, S. Diele, C. Tschierske, *Chem. Eur. J.* **2001**, *7*, 2245-2253.
- [78] C. Backes, T. Schunk, F. Hauke, A. Hirsch, *J. Mater. Chem.* **2011**, *21*, 3554-3557.
- [79] S. Rehm, V. Stepanenko, X. Zhang, T. H. Rehm, F. Würthner, *Chem. Eur. J.* **2010**, *16*, 3372-3382.
- [80] J. K. Gallaher, E. J. Aitken, R. A. Keyzers, J. M. Hodgkiss, *Chem. Commun.* **2012**, *48*, 7961-7963.
- [81] T. Heek, F. Würthner, R. Haag, *Chem. Eur. J.* **2013**, *19*, 10911-10921.
- [82] S. M. Bachilo, M. S. Strano, C. Kittrell, R. H. Hauge, R. E. Smalley, R. B. Weisman, *Science* **2002**, *298*, 2361-2366.
- [83] A. Setaro, *J. Phys.: Condens. Matter* **2017**, *29*, 423003.
- [84] S. Reich, C. Thomsen, J. Maultzsch, *Carbon Nanotubes: Basic Concepts and Physical Properties*, Wiley-VCH, Weinheim, **2004**

- [85] D. Roxbury, P. V. Jena, R. M. Williams, B. Enyedi, P. Niethammer, S. Marcet, M. Verhaegen, S. Blais-Ouellette, D. A. Heller, *Sci. Rep.* **2015**, *5*, 14167.
- [86] C. Roquelet, J.-S. Lauret, V. Alain-Rizzo, C. Voisin, R. Fleurier, M. Delarue, D. Garrot, A. Loiseau, P. Roussignol, J. A. Delaire, E. Deleporte, *ChemPhysChem* **2010**, *11*, 1667-1672.
- [87] Z. Sun, Z. Liu, J. Meng, J. Meng, J. Duan, S. Xie, X. Lu, Z. Zhu, C. Wang, S. Chen, H. Xu, X.-D. Yang, *PLOS ONE* **2011**, *6*, e21073.
- [88] J. Wang, P. Sun, Y. Bao, J. Liu, L. An, *Toxicol. In Vitro* **2011**, *25*, 242-250.
- [89] X. Shi, B. Sitharaman, Q. P. Pham, P. P. Spicer, J. L. Hudson, L. J. Wilson, J. M. Tour, R. M. Raphael, A. G. Mikos, *J. Biomed. Mater. Res., Part A* **2008**, *86A*, 813-823.
- [90] H. Wang, W. Zhou, D. L. Ho, K. I. Winey, J. E. Fischer, C. J. Glinka, E. K. Hobbie, *Nano Lett.* **2004**, *4*, 1789-1793.
- [91] Z. Liu, S. Tabakman, K. Welsher, H. Dai, *Nano Res.* **2009**, *2*, 85-120.
- [92] M. Berna, D. Dalzoppo, G. Pasut, M. Manunta, L. Izzo, A. T. Jones, R. Duncan, F. M. Veronese, *Biomacromolecules* **2006**, *7*, 146-153.
- [93] S. Ahn, E. Seo, K. Kim, S. J. Lee, *Sci. Rep.* **2013**, *3*, 1997.
- [94] Y. Xiao, T. Gong, S. Zhou, *Biomaterials* **2010**, *31*, 5182-5190.
- [95] D. W. Dunne, D. Resnick, J. Greenberg, M. Krieger, K. A. Joiner, *Proc. Natl. Acad. Sci. U. S. A.* **1994**, *91*, 1863-1867.